arXiv:hep-ph/0206027v1 4 Jun 2002

UNICAL-TH 06/4
UAB-FT-529
June 2002

EXPLICIT MODEL REALIZING PARTON-HADRON DUALITY ⋆

R. Fiore[a†], A. Flachi[b◇], L.L. Jenkovszky[c‡], A.I. Lengyel[d§], V.K. Magas[c,e∗]

[a] *Dipartimento di Fisica, Università della Calabria & INFN-Cosenza, I-87036 Arcavacata di Rende, Cosenza, Italy*

[b] *IFAE, Universidad Autònoma de Barcelona, 08193 Bellaterra, Barcelona, Spain*

[c] *Bogolyubov Inst. for Theor. Phys., Ac. of Sciences of Ukraine UA-03143 Kiev, Ukraine*

[d] *Institute of Electron Physics, Universitetska 21, UA-88000 Uzhgorod, Ukraine*

[e] *Center for Physics of Fundamental Interactions (CFIF), Physics Department, Instituto Superior Tecnico, Av. Rovisco Pais, 1049-001 Lisbon, Portugal*

Abstract

An explicit model realizing parton-hadron duality and fitting the data is suggested. Complex nonlinear Regge trajectories are important ingredients of the model. The inclusion of Δ and N^* trajectories should account for all resonances in the direct channel. The exotic trajectory is responsible for the smooth background.

⋆ *Work supported in part by the Ministero dell'Istruzione, dell'Università e della Ricerca (MIUR) and by the INTAS*

† *e-mail address:* FIORE@CS.INFN.IT
‡ *e-mail address:* JENK@GLUK.ORG
◇ *e-mail address:* FLACHI@IFAE.ES
§ *e-mail address:* SASHA@LEN.UZHGOROD.UA
∗ *e-mail address:* VLADIMIR@CFIF.IST.UTL.PT

1 Introduction

The photoabsorption cross section in the resonance region has been studied in a large number of papers [1, 2, 3, 4, 5] (for a comprehensive review see Ref. [6]). There are nearly 20 resonances in the $\gamma^* p$ system in the region between the pion-nucleon threshold and below 2 GeV, but only a few of them can be identified more or less unambiguously. One reason is that they overlap and compete with changing Q^2 and the other is the uncertainty due to the background. Therefore, instead of identifying each resonance, one considers three maxima above the elastic scattering peak, corresponding to some "effective" resonance contributions. Most of the data come from SLAC and have been compiled by Stoler [7]. The first maximum is due to the isolated $\Delta(1232)$ resonance. The second resonance region is dominated by two strong negative-parity states, the $D_{13}(1520)$ and the $S_{11}(1535)$. At low Q^2 (< 1 GeV^2) the $D_{13}(1520)$ dominates, whereas at high Q^2 (~ 3 GeV^2) there is some evidence that the $S_{11}(1535)$ becomes dominant. The relative strength of the other states is not well determined, especially at increasing Q^2. For example, in the fits for $Q^2 > 4$ GeV^2 it is usually assumed that only $S_{11}(1535)$ contributes to the second resonance, eventually corrected for $Q^2 \leq 4$ GeV^2 to subtract the contribution from the $D_{13}(1520)$. In the third resonance region, the strongest excitation at low Q^2 is the $F_{15}(1680)$ state. Although it is assumed that this remains one state, it is possible that several states contribute strongly at high Q^2. All the fits include a state at $W = 1440$ MeV, corresponding to the possible location of the $P_{11}(1440)$, but these fits do not exhibit any positive contribution from this state. Ultimately, in most of the phenomenological fits only three peaks are included, namely those at $W \sim 1232$, 1535 and 1680 MeV.

The standard approach to the phenomenological analysis of the data is that developed in Ref. [1] and still widely used. Ignoring the (relatively small) longitudinal component of the total cross section, one writes the contribution of the three

for the Δ resonance and non-relativistic formulae for the the second and the third resonance regions. [1]

The above resonance contribution is appended by a smooth background, parametrized as

$$\sigma_T^{bg} = \sum_{n=1}^{3} C_n(Q^2)(W - W_{th})^{n-1/2}, \tag{1}$$

where the square-root term $(W - W_{th})^{1/2}$ takes into account the behavior of non-resonant pion production at the threshold $W_{th} = m_p + m_\pi$ (m_p is a proton mass). The coefficients $C_n(Q^2)$ are polynomials of Q^2: $C_n(Q^2) = \sum_{j=0}^{4} C_{nj} Q^{2j}$. A detailed analysis of the SLAC data along these lines can be found e.g. in [4, 8].

Systematic theoretical studies of the subject, including the helicity structure of the amplitude, the threshold- and the QCD-motivated asymptotic behavior of the form factors can be found in the papers by Carlson and co-authors [9, 10] (see also Ref. [11]). Spin structure functions (SF's) were studied in Ref. [12].

Recent results from JLab (CEBAF) [13] renewed the interest in the subject [14, 15, 16] and they call for a more detailed phenomenological analysis of the data and a better understanding of the underlying dynamics.

In the present paper we develop further the arguments presented in Refs. [17, 18, 19] and earlier works cited therein. The basic idea in our approach is to use the off-mass-shell continuation of the dual amplitude with nonlinear complex Regge trajectories. These trajectories play a crucial role in the dynamics of the strong interactions. Actually, the trajectories can be considered as the basic dynamical variables, replacing the usual Mandelstam variables s, t and u. In particular, their

[1] We remind that this is a phenomenological description since the Breit-Wigner formulae are applied to a peak created by a superposition of resonances rather than to a single resonance.

form determines completely the spectrum of resonances (see e.g. Ref. [20]). The parameters of the trajectories can be fitted independently of the masses and widths of the known resonances, therefore, in principle, they reflect more adequately the position of the peaks in ep scattering, formed by the interplay of different resonances. In concentrating on this aspect of the dynamics, we leave more freedom to the choice of the Q^2-dependent form factors. We start with a simplified model, disregarding the helicity structure of the amplitudes. We ignore the relatively small (and poorly known) contribution from the cross sections involving longitudinally polarized photons, σ_L . In doing so, we anticipate the connection [17] with the small-x (high-energy) domain, where these simplifications are commonly accepted.

Apart from the above-mentioned details, there is an important problem in the Q^2-dependence, namely the asymptotic behavior of the form factors, usually related to the quark counting rules. While the validity of these rules for elastic form factors leaves a little doubt, they may get modified for the transition form factors. Moreover, in our approach a new type of form factors, generalizing the concept of inelastic form factors, appears. These new form factors correspond to the transition of the nucleon to a baryon trajectory, with a sequence of nucleon resonances on it. It follows from dual models (see Section 3 and Ref. [17]) that the powers of these form factors increase with the spin of the excited state.

We adopt the two-component picture of strong interactions [21], according to which direct-channel resonances are dual to cross-channel Regge exchanges and the smooth background in the $s-$channel is dual to the Pomeron exchange in the $t-$channel. As explained in Ref. [17], the background corresponds in a dual model to a pole term with an exotic trajectory that does not produce any resonance.

To summarize the philosophy of the present paper (for a related approach see Ref. [22]), we believe that the mechanism of virtual photoproduction on nucleons is not much different from that in purely hadronic processes. Since at intermediate energies the entire nondiffractive part of the hadronic amplitude is saturated by direct-channel resonances, by duality they determine completely the dynamics of the reaction. By expressing the inelastic electron scattering cross section through the imaginary part of the virtual Compton scattering amplitude, it is reasonable to assume that a resonance model will work for virtual Compton scattering equally well as for pion-nucleon scattering, i.e. both are saturated by the contribution of many overlapping resonances. The crucial question is the spectrum of these resonances, connected with the form of nonlinear, complex Regge trajectories.

The paper is organized as follows: the kinematics of eN scattering and the relevant notation is described in Section 2. The properties of Regge trajectories, which constitute a basic ingredient of our model, are discussed in Section 3. The model for the nucleon structure function is presented in Section 4 and the fitting procedure and comparison with data is discussed in Section 5. Sections 6 and 7 are devoted to analytical and numerical tests of parton-hadron duality. Finally, we draw our conclusions in Section 8.

2 Notation, kinematics and observables

We study inclusive electron-nucleon scattering shown in Fig. 1. The scattered electron, entering into the process with energy E, emerges with energy E' at an angle θ with respect to the initial direction. The four-momentum transferred by the virtual photon from the electron to the nucleon is $q = k - k' = -Q^2$, where k

and k' are the four-momenta of incoming and outgoing electrons, respectively. The energy transferred between the electron and the nucleon (or the energy lost by the electron) is

$$\nu = \frac{pq}{m} = E - E', \tag{2}$$

where p is the four-momentum of the target nucleon of mass m. The invariant squared mass of the recoiling system (hadronic final state) is

$$W^2 = (p+q)^2 = m^2 + 2m\nu - Q^2. \tag{3}$$

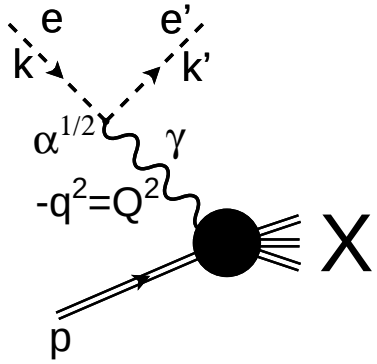

Figure 1: Kinematic of deep inelastic scattering.

An experimentally measurable quantity in the the reaction $e(k)+N(p) \rightarrow e'(k')+X$ is the differential cross section (see e.g. Ref. [23])

$$\frac{d^2\sigma^{\gamma^* p}}{d\Omega dE'} = \Gamma(\sigma_T + \epsilon\sigma_L), \tag{4}$$

where

$$\Gamma = \frac{\alpha K}{2\pi^2 Q^2}\frac{E'}{E}\frac{1}{1-\epsilon}, \tag{5}$$

with $K = (W^2 - m^2)/(2m)$ and

$$\epsilon = \left(1 + 2\frac{\nu^2 + Q^2}{Q^2}\tan^2\frac{\theta}{2}\right)^{-1} \tag{6}$$

or

$$\frac{d^2\sigma^{\gamma^* p}}{d\Omega dE'} = \Gamma\sigma_T(1+\epsilon R). \tag{7}$$

The ratio $R = \sigma_L/\sigma_T$ relates the transverse component of the cross section, σ_T, to the longitudinal component, σ_L. The structure function F_2 can be expressed in terms of the differential cross section and R as

$$F_2 = \frac{d^2\sigma^{\gamma^* p}}{d\Omega dE'}\frac{1+R}{1+\epsilon R}\left[\frac{K\nu}{4\pi^2\alpha}\frac{1}{\Gamma}\frac{1}{1+\frac{\nu^2}{Q^2}}\right] , \tag{8}$$

where the kinematics is given by the term in square brackets.

Phenomenological parameterizations for the quantity R exist in the literature [5], but in this paper, as we are ignoring the spin structure, we shall put $R = 0$.

The central object of the present study is the nucleon SF, uniquely related to the photoproduction cross section by

$$F_2(x,Q^2) = \frac{Q^2(1-x)}{4\pi\alpha(1+\frac{4m^2x^2}{Q^2})}\sigma_t^{\gamma^* p}(s,Q^2) , \tag{9}$$

where total cross section, $\sigma_t^{\gamma^* p}$, is the imaginary part of the forward Compton scattering amplitude, $A(s,Q^2)$,

$$\sigma_t^{\gamma^* p}(s) = \mathcal{I}m\ A(s,Q^2) . \tag{10}$$

The center of mass energy of the $\gamma^* p$ system, the negative squared photon virtuality Q^2 and the Bjorken variable x are related by

$$s = W^2 = Q^2\frac{(1-x)}{x} + m^2, \tag{11}$$

Instead of W^2, we use the Mandelstam variable s, typical of hadronic reactions.

3 Nonlinear complex Regge trajectories. Direct-channel resonances and background

The SF is related via Eq. (9) to the total cross section, or the imaginary part of the forward Compton scattering amplitude, Eq. (10). The latter, on the other hand, is related by unitarity to the sum of all possible intermediate states, as shown in Fig. 2 (see e.g. Ref. [24]). One should distinguish between cross sections summed over a limited number of nuclear excitations [1, 7], $\sigma_{\gamma N \to R_i}$ and the total cross section of virtual forward Compton scattering, related to the SF, including by unitarity all possible intermediate states allowed by energy and quantum number conservation.

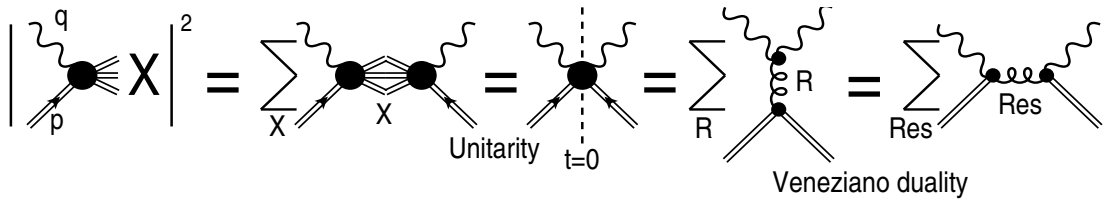

Figure 2: According to the Veneziano (or resonance-Reggeon) duality a proper sum of either t-channel or s-channel resonance exchanges accounts for the whole amplitude.

The correct way to fully account for all possible intermediate states in the resonance region is in terms of the s-channel Regge trajectories, which automatically include the huge number of resonances as recurrences, appearing on the trajectories [19]. This is an economic way to take into account the whole sequence of nucleon excitations, lying on a single trajectory. This is more than a mere technical simplification: Regge trajectories are basic building blocks in dual models. The kinematical variables enter through Regge trajectories, which thus play the role of dynamical variables. Now, since the behavior of the Regge trajectories is assumed to be known

in the whole range of their variation, the resulting behavior of the SF can be thus extrapolated towards small x, well beyond the resonance region.

The dynamics of the resonance formation is intimately related to the form of the Regge trajectories. Their linear rise is a widely accepted approximation. It is based on the observed spectrum of resonance masses and was supported by narrow resonance dual models and their mechanical analogues, such as the harmonic oscillator or relativistic strings.

In fact, linear trajectories contradict both the theory and the data: analyticity requires the presence of threshold singularities in the trajectories, while their asymptotic behavior is also constrained by an upper bound on their real part. The finite widths of resonances also require the presence of a nonvanishing imaginary part in the trajectories.

Explicit models of Regge trajectories realizing the above requirements were studied in a number of papers (see Ref. [20] and references therein). The main feature of these trajectories is that the number of resonances is finite (due to an upper limit on their real part, determined by fits to the data), as illustrated in Fig. 3. A particularly simple model is based on a sum of square roots

$$\alpha(s) = \alpha_0 + \sum_i \gamma_i \sqrt{s_i - s}, \tag{12}$$

where the lightest threshold gives rise to the imaginary part while the heaviest one promotes the nearly linear rise of the real part at small and intermediate s. To simplify the calculations, in a limited range of s, the heaviest threshold can be approximated by a linear term, hence the expression (12) for the trajectory can be

written as

$$\alpha(s) = \alpha_0 + \alpha_1 s + \alpha_2(\sqrt{s_0} - \sqrt{s_0 - s}), \tag{13}$$

where s_0 is the lightest threshold, $s_0 = (m_\pi + m_p)^2 = 1.14$ GeV^2 in our case. Beyond the threshold, the real part of this trajectory is $\mathcal{R}e\ \alpha(s) = \alpha_0 + \alpha_2\sqrt{s_0} + \alpha_1 s$, while its imaginary part is $\mathcal{I}m\ \alpha(s) = \alpha_2\sqrt{s - s_0}$.

Large-angle scaling behavior of the hadronic amplitudes constrains [26] the asymptotic (far away from the resonance region) behavior of the trajectories by a logarithm

.

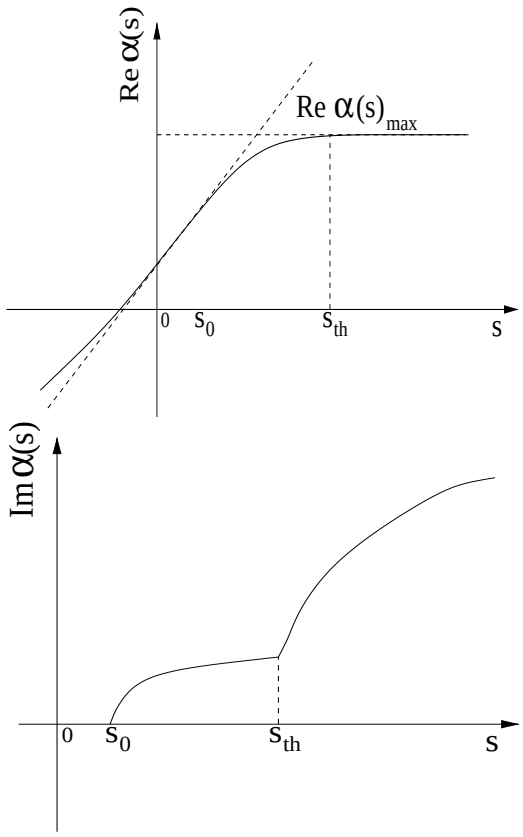

Figure 3: Typical behavior of the real and imaginary parts of an analytic model of the Regge trajectory [25]. The (nearly) smooth behaviour results from the smearing of several additive thresholds in Eq. (12).

In $\gamma^* p$ scattering only N (isospin 1/2) and Δ (isospin 3/2) resonances contribute in the s channel. The latest Review of Particle Physics [27] quotes about 14 N's whose "existence is certain or very likely certain" plus 8 N's whose "evidence is fair or poor") and 10 "certain or likely certain" (plus 12 "fair or poor") Δ's. Most, if not all of the above two dozen (almost) certain resonances - among them the "prominent" ones mentioned in the Introduction - contribute, with different weights, to the the $\gamma^* N$ total cross section or to the nucleon SF. It is clear that a systematic account for all these resonances (plus those to be confirmed) is not an easy task. A much more economic way is to introduce the whole sequence of recurrences. As well as generalizing the concept of a resonance (a Regge trajectory realizes the analytic continuation of the discrete resonance spin and is an indispensable ingredient of dual models!), the trajectory may also be used to classify the resonances by eliminating some candidates and predicting others. The above resonances lie on several positive- and negative-parity N and Δ trajectories.

The classification of meson and baryon resonances on the basis of Regge recurrences of SU(3) multiplets was extensively studied in the late sixties (see e.g. Ref. [24]). A nontrivial model for meson Regge trajectories with the limited real part was suggested in a recent paper [20]. Anticipating analogous new results for baryon trajectories, below we shall use a simple model, based on the ideas introduced above and fitted to the three "prominent" resonances, seen in ep scattering.

4 The model

To illustrate these ideas, we start with a simplified model, in which we disregard the helicity structure of the scattering amplitude and relevant selection rules, con-

centrating on the role of the Regge trajectories, analyticity and duality. Their role was treated in a number of papers [9] (recently in Ref. [28]).

In the dual-Regge approach [17, 18, 19] the Compton scattering can be viewed as an off-mass shell continuation of a hadronic reaction, dominated in the resonance region by non-strange (N and Δ) baryon trajectories. The scattering amplitude follows from the pole decomposition of a dual amplitude [17]

$$A(s,Q^2)\Big|_{t=0} = norm \sum_{i=N_1^*,N_2^*,\Delta,E} A_i \sum_{n=n_i^{min}}^{n_i^{max}} \frac{f_i(Q^2)^{2\left(n-n_i^{min}+1\right)}}{n-\alpha_i(s)} \ , \qquad (14)$$

where i runs over all the trajectories allowed by quantum number exchange, $norm$ and A_i's are constants, $f_i(Q^2)$'s are the form factors. These form factors generalize the concept of inelastic (transition) form factors to the case of continuous spin, represented by the direct-channel trajectories. The n_i^{min} refers to the spin of the first resonance on the corresponding trajectory i (it is convenient to shift the trajectories by 1/2, therefore we use $\alpha_i = \alpha_i^{phys} - 1/2$, which due to the semi-integer values of the baryon spin leaves n in Eq. (14) integer). The sum over n goes with step 2 (in order to conserve parity).

It follows from Eq. (14) that

$$\mathcal{I}m\ A(s,Q^2) = norm \sum_{i=N_1^*,N_2^*,\Delta,E} A_i \sum_{n=n_i^{min}}^{n_i^{max}} \frac{[f_i(Q^2)]^{2\left(n-n_i^{min}+1\right)}\mathcal{I}m\ \alpha_i(s)}{(n-\mathcal{R}e\ \alpha_i(s))^2+(\mathcal{I}m\ \alpha_i(s))^2} \ . \qquad (15)$$

Eqs. (14, 15) have a factorized form, a product of vertices (two identical form factors) times the propagator. Each term in Eq. (15) resembles that of a Breit-Wigner formula with a resonance mass $s_n = (n-\alpha_0-\alpha_2\sqrt{s_0})/\alpha_1$ ($\mathcal{R}e\ \alpha(s_n) = n$) and an energy-dependent width given by $\mathcal{I}m\ \alpha(s_n)/\alpha_1$ of the trajectory. The factor $(n-\alpha(s))^{-1}$ is typical of the dual-Regge approach [17].

The first three terms in (15) are the non-singlet, or Reggeon contributions with the N^* and Δ trajectories in the s-channel, dual to the exchange of an effective bosonic trajectory (essentially, f) in the t-channel, and the fourth term is the contribution from the smooth background, modeled by a non-resonance pole term with an exotic trajectory $\alpha_E(s)$, dual to the pomeron (see Ref. [17]). As argued in Ref. [17], only a limited number, $\mathcal{N}$, of resonances appear on the trajectories, for which reason we tentatively set $\mathcal{N} = 3$, i.e. one resonance on each trajectories ($N_1^*,\ N_2^*,\ \Delta$). We tried also with higher values of $\mathcal{N}$, up to $\mathcal{N} = 10$, but our analyses shows that $\mathcal{N} = 3$ is a reasonable approximation – even if additional peaks appear, they are suppressed with respect to the dominant one (first on each trajectory), because of the Q^2-behaviour of the form factors. Thus, the limited (small) number of resonances contributing to the cross section results not only from the termination of resonances on a trajectory but even more due to the strong suppression coming from the numerator (increasing powers of the form factors).

Since, by definition, the smooth background does not show any resonance, here we keep only one term in the sum (for more details see [17, 18, 19] and references therein).

By inserting in Eq. (15) the relevant baryonic trajectories, we include all possible electromagnetic transitions from a nucleon to its excitations. There are, however, selection rules, enhancing some and suppressing others. This effect will be taken into account by our phenomenological fits to the data.

As discussed above the nonlinear behaviour of the trajectories, especially the boundedness of their real part, is a crucial feature of our dual model. For practical reasons we have replaced the formal condition $\mathcal{R}e\ \alpha(s) < const$ by a finite sum

in Eq. (15), introducing a linear term in the baryon trajectory to approximate the contribution from heavy thresholds (see Eq. (13)).

We have fitted the parameters of the baryon trajectories, given by Eq. (13), such as to reproduce the experimental masses and widths of the following resonances:

Resonance	$I\ \left(J^P\right)$	M, GeV	Γ, GeV
$\Delta(1236)$	$\frac{3}{2}\left(\frac{3}{2}^+\right)$	1.230	0.115
$N^*(1520)$	$\frac{1}{2}\left(\frac{3}{2}^-\right)$	1.515	0.11
$N^*(1680)$	$\frac{1}{2}\left(\frac{5}{2}^+\right)$	1.690	0.12

We end up with the following trajectories:

$$\alpha_{N_1^*}(s) = -0.8377 + 0.95s + 0.1473(\sqrt{s_0} - \sqrt{s_0 - s}) \ , \tag{16}$$

$$\alpha_{N_2^*}(s) = -0.37 + 0.95s + 0.1471(\sqrt{s_0} - \sqrt{s_0 - s}) \ , \tag{17}$$

$$\alpha_{\Delta}(s) = 0.0038 + 0.85s + 0.1969(\sqrt{s_0} - \sqrt{s_0 - s}) \ . \tag{18}$$

We take only one resonance on each trajectory, so the sum over n in Eq. (15) reduces to one term, i.e. $n_i^{max} = n_i^{min}$ for all three baryon trajectories as well as for the exotic one.

We take the exotic trajectory in the form

$$\alpha_E(s) = \alpha_E(0) + \alpha_{1E}(\sqrt{s_E} - \sqrt{s_E - s}), \tag{19}$$

where the intercept $\alpha_E(0)$, α_{1E} and the effective exotic threshold s_E are free parameters. As a first approximation we can assume the following expression for the exotic trajectory [17]:

$$\alpha_E(s) = 0.5 + 0.12(\sqrt{s_E} - \sqrt{s_E - s}) \ , \tag{20}$$

where $s_E = 1.145^2$ GeV^2. As we said above, we take only one term from exotic trajectory. n_E^{min} is the first integer larger then $Max(\mathcal{R}e\ \alpha_E)$ (to make sure there are no resonances on the exotic trajectory); in our case $n_E^{min} = 1$.

In dual models, the numerator in Eq. (15) contains powers of the intercepts of the t-channel trajectories, $\alpha_t^n(0)$ and/or powers of a parameter g that in Ref. [17] was assumed to be Q^2-dependent by matching the Regge behaviour and the Bjorken scaling. As it was mentioned before, here we invert the problem and, in accordance with the factorization properties of the amplitude, we multiply the resonance propagators by the product of the inelastic form factors (to be later identified with the parameters of the dual model [17]).

To start with we use the simplest, dipole model for the form factors, disregarding the spin structure of the amplitude and the difference between electric and magnetic form factors:

$$f_i(Q^2) = \frac{1}{(1 + \frac{Q^2}{Q^2_{0,i}})^2} \ . \tag{21}$$

where $Q^2_{0,i}$ are scaling parameters.

From Eq. (15) one can immediately guess that the first resonance on each trajectory, Δ, N_1^*, N_2^* or E, will become dominant over the subsequent ones with increasing Q^2 due to the power behavior of the form factors. The relative growth of these three terms will depend on the scaling factor $Q^2_{0,i}$. Therefore we choose $Q^2_{0,E} > Q^2_{0,N_2^*} > Q^2_{0,N_1^*} > Q^2_{0,\Delta}$ in order to satisfy the experimentally observed behaviour of these terms, for example, the rise of the background contribution with respect to the resonance one with increasing Q^2; the relative growth of the N_1^* and N_2^* peaks with respect to the Δ peak.

5 Fits to the SLAC and JLab data

In this Section we present a numerical analysis of our model based on the experimental data from SLAC [7] and JLAB [29][2].

Before displaying the results of our fits, it is instructive to illustrate the ideas behind our study, in order to make the following results physically more transparent.

We are dealing with a set of 704 experimental points for 7 different values of Q^2: 0.45, 0.85, 1.4, 1.7, 2.4, 3.0, 3.3 GeV^2. A first rough fit when the whole data-set is taken into account produces $\chi^2_{d.o.f.} \propto 10^4$. This has to do with the fact that the set of experimental data is not homogeneous, i.e. points at low s (high x) are given with very small experimental errors, thus "weighting" the fitting procedure not uniformly. This forced us to make a preselection in the initial data-set by removing points with $\chi^2_{red} \leq 1000$. Below we will be considering the leftover 634 data points (90% of the original data-set), although all the experimental points are presented in the Figures.

As we have seen in Section 4, our model consists of the sum of the contributions from three resonances (N_1^*, N_2^*, Δ), which give the dominant contribution to the structure functions, plus an exotic background, that we treat effectively. The first approach to the fitting procedure consists in fixing parameters of the trajectories for the resonances, in order to reproduce the correct masses and widths, leaving the four scaling constants Q_i^2, four factors A_i and the parameters of the exotic trajectories to be fitted to the data. The results are shown in Table 1 (first coloumn) and the plots of the SF against x are presented in Fig. 7 (dashed-dotted lines).

Although the agreement with the experimental data seems not to be good ($\chi^2_{red} =$

[2]We are grateful to M.I. Niculescu for making her data compilation available to us.

28.29), there is a number of features which we could introduce in order to improve the model.

A first important aspect is to account for the large number of resonances (about 20) present in the energy range under investigation, which overlap, as noted in Section 3. For this reason we consider the dominant resonances (N_1^*, N_2^* and Δ) as "effective" contributions to the SF. In other words we require that they mimic the contribution of the dominant resonances plus the large number of subleading contributions, which, together, fully describe the real physical system.

A way of doing this is to consider corrections to the model as explained in the following. If we denote the structure function as $F(\alpha, x, Q^2)$, where α represents generically the trajectories' parameters, the contribution from the subleading resonances can be introduced as corrections to the α's. Thus, the "effective" SF becomes a function of some corrected trajectories $F(\alpha + \delta\alpha, x, Q^2)$, where α, represents the physical value and $\delta\alpha$ the correction which accounts for the subleading resonances. However, due to the fact that the physical resonances give the dominant contribution, we expect this departure not to be large.

In the light of these considerations, we have refitted the data, allowing the baryon trajectories parameters to vary. The resulting parameters of such a fit are reported in Table 1 (second coloumn). It is worth noting that although the range of variation was not restricted, the new parameters of the trajectories stay close to their physical values, showing stability of the fit and thus reinforcing our previous considerations. From the relevant plots, shown in Fig. 7 with full lines, one can see that the improvement is significant, although agreement is still far from being perfect ($\chi^2_{d.o.f.} = 11.6$).

Another important ingredient to be introduced in the model is spin. This changes the form factors in a non-trivial way, thus complicating the Q^2-dependence of the SF's (see Ref. [28] for a recent treatment of the problem). These corrections have not yet been included in our study and might be responsible for relatively poor agreement with data. We hope to address this problem in a forthcoming work.

One may also ask the question of how good the dipole expression for the form factors, Eq. (21) does work. To answer this question we performed the fit letting the powers of the $1/(1+Q^2/Q^2_{0,i})$ in Eq. (21) free to vary. The results show that second power is a good approximation - powers change only by about 5%. As we shall see in the next Section, the dipole approximation deteriorates towards large values of Q^2. This phenomenon may be partly due to the spin effects, ignored in the present model.

6 Parton-hadron duality: a numerical tests

In order to quantify the validity of the quark-hadron duality, it is customary (see e.g. Ref. [8]) to compare the Q^2-behaviour of the following quantities:

$$I_{Bj}(Q^2) = \int_{s_{th}}^{s_{max}} ds\ F_2^{Bj}\ , \tag{22}$$

$$I_{Model}(Q^2) = \int_{s_{th}}^{s_{max}} ds\ F_2^{Model}\ , \tag{23}$$

where the lower integration limit is fixed to $s_{th} = s_0$ and the upper integration limit, s_{max}, is varied within the range $3 - 25$ GeV^2.

Here F_2^{Model} is our model, given by Eqs. (9), (10), (15) and F_2^{Bj} is a "scaling curve", i.e. a phenomenological parameterizations of the SF exhibiting Bjorken

scaling and fitting the data. We have chosen the parameterizations studied in Ref. [30], which we report for the convenience of the reader,

$$F_2^{Bj}(x,Q^2) = F_S(x,Q^2) + F_{NS}(x,Q^2) \ , \tag{24}$$

where

$$F_{NS}(x,Q^2) = D \cdot x^{1-\alpha_R} \cdot (1-x)^{n(Q^2)} \cdot \left(\frac{Q^2}{Q^2+b}\right)^{\alpha_R} \ , \tag{25}$$

$$n(Q^2) = \frac{3}{2} \cdot \left(1 + \frac{Q^2}{Q^2+c}\right) \ . \tag{26}$$

The singlet component of the SF, corresponding to a multipole (single+double+triple) Pomeron is a sum of logarithms:

$$\begin{array}{c} F_S(x,Q^2) = Q^2 \, [\, A \left(\frac{a}{a+Q^2}\right)^{\alpha} + B \left(\frac{a}{a+Q^2}\right)^{\beta} \log\left(\frac{Q^2}{x}\right) + \\ C \left(\frac{a}{a+Q^2}\right)^{\gamma} \log^2\left(\frac{Q^2}{x}\right) \,] \, (1-x)^{n(Q^2)+4} \ . \end{array} \tag{27}$$

The values of the parameters, $A,\ B,\ C,\ D,\ a,\ b,\ c,\ \alpha,\ \beta,\ \gamma$ and α_R can be found in [30]. The corresponding curves are presented by dashed lines in Fig. (7).

The quantity of interest is the so called duality ratio given by

$$\mathcal{I}(Q^2) = \frac{I_{model}(Q^2)}{I_{Bj}(Q^2)} \ . \tag{28}$$

Its deviation from unity is indicative of any violation of parton-hadron duality. We compute numerically this quantity, using values of the second set of parameters (Table (1), second coloumn) and show the result in Fig. 4.

One can see from Fig. 4 that for a short interval of integration our model strongly overshoots the "scaling curve", since in this region we have strongly peaked resonances. For s_{max} larger than 5 GeV^2 this effect saturates. As we tend to the large Q^2 region our model starts to underestimate the "scaling curve". It was stressed in Ref. [30] that the scaling curve itself starts to overestimate the data for

$Q^2 > 15 - 20$ GeV^2. The strong decrease of $\mathcal{I}(Q^2)$ for high Q^2 is partly due to this fact. The subplot shows that in the Q^2 interval of interest the $\mathcal{I}(Q^2)$ deviates from 1 by 20-40%.

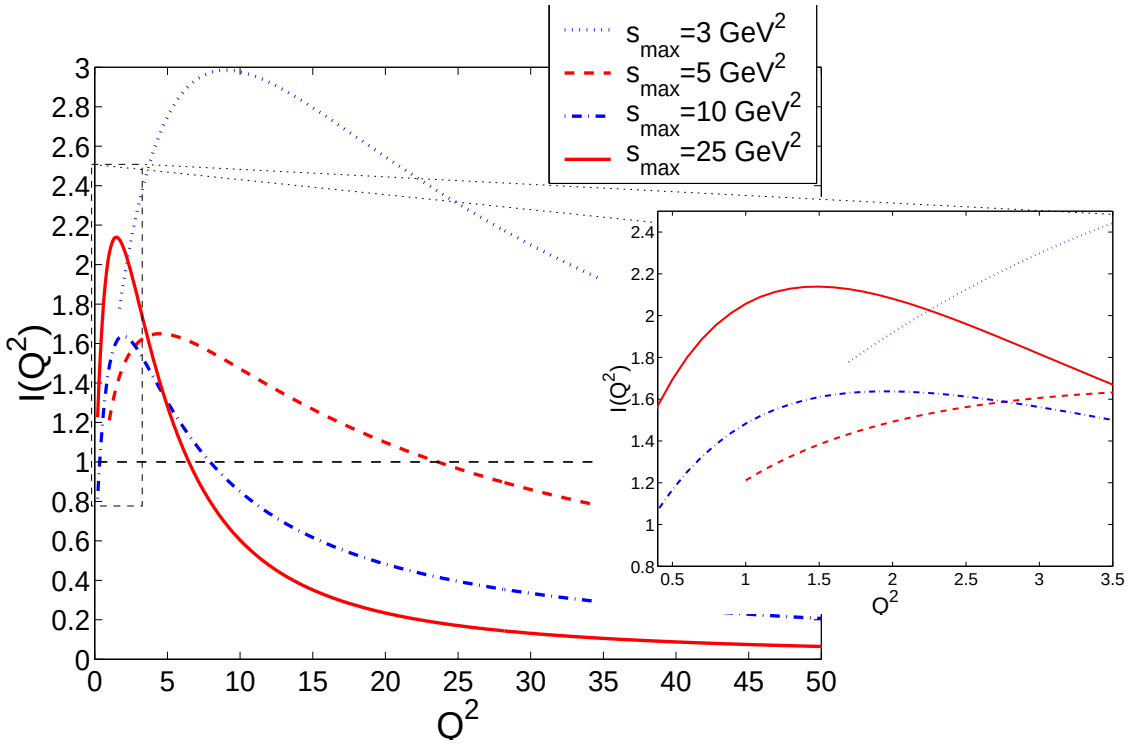

Figure 4: Parton-hadron duality test for different s_{max}.

We have calculated also the Q^2-dependent ratio of the resonance to background components of the SF at three fixed values x, namely at three physical resonance peaks, $s_{N_1^*}$, $s_{N_2^*}$, s_Δ, for the fit with fixed physical baryon trajectories and at effective resonance peaks, $s^{eff}_{N_1^*} = 1.494^2$ GeV^2, $s^{eff}_{N_2^*} = 1.690^2$ GeV^2, $s^{eff}_{\Delta} = 1.22^2$ GeV^2, for the fit with free baryon trajectories[3]. On this plot the "background" for the selected resonance consists of three parts, i.e. contribution from the exotic trajectory (usual background term) and contributions from the two other resonances. The results

[3]Notice that the position of the N_2^* resonance remains the same for the effective trajectory. Others also do not change much.

are shown in Fig. 5. One may see that for N_2^* and for N_1^* for $Q^2 > 1.5$ GeV^2 the "background" contributes more than the resonant term itself.

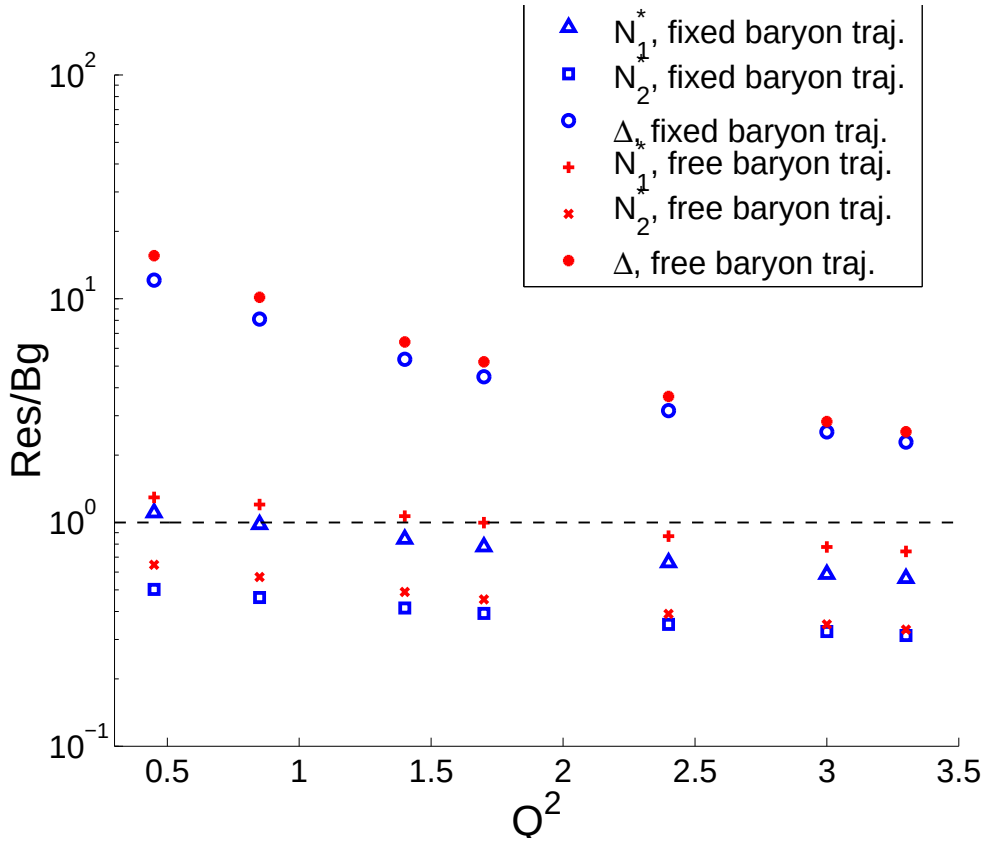

Figure 5: The ratio of the resonance to background components of the SF at the resonance peaks. See text for more details.

7 Parton-hadron duality: an analytical tests

Consider now the behaviour of $F_2(x, Q^2)$ at large x when s is kept in the resonance region. Let us remind the reader that x, Q^2 and s are related by Eq. (11) with $m = m_p$. Thus, each term in the rhs of Eq. (15), using Eqs. (9, 10) looks like

$$F_2(x,Q^2)_{i,n} = \frac{Q^2(1-x)}{4\pi\alpha(1+\frac{4m_p^2x^2}{Q^2})} \frac{norm\ A_i}{(1+\frac{Q^2}{Q^2_{0,i}})^{4(n-n_i^{min}+1)}}$$

$$\cdot \frac{\mathcal{I}m\ \alpha_i(s)}{(n - \mathcal{R}e\ \alpha_i(s))^2 + (\mathcal{I}m\ \alpha_i(s))^2}\ . \tag{29}$$

In our case, since we consider only one resonance on each trajectory, we have

$$F_2(x,Q^2)_{i,n} \propto \frac{1}{(1+\frac{Q^2}{Q^2_{0,i}})^4}\ . \tag{30}$$

In the limit of x going to 1 and s in the resonance region ($1 - 4$ GeV^2), $Q^2 = x(s-m_p^2)/(1-x)$ is much larger than s and $Q^2_{0,i}$, which are of the same order. Therefore

$$\frac{1}{(1+\frac{Q^2}{Q^2_{0,i}})^4} \approx \frac{(1-x)^4}{\left(\frac{x(s-m_p^2)}{Q^2_{0,i}}\right)^4}\left(1 - 4\frac{Q^2_{0,i}}{Q^2} + O\left(\frac{1}{Q^4}\right)\right)\ . \tag{31}$$

Using $x = Q^2/(Q^2+s-m_p^2) = 1-(s-m_p^2)/Q^2$ we can go one step further:

$$\frac{1}{(1+\frac{Q^2}{Q^2_{0,i}})^4} \approx \frac{(1-x)^4}{\left(\frac{(s-m_p^2)}{Q^2_{0,i}}\right)^4}\left(1 - 4\frac{Q^2_{0,i}+s-m_p^2}{Q^2} + O\left(\frac{1}{Q^4}\right)\right)\ . \tag{32}$$

Thus

$$F_2(x,Q^2) \approx norm \sum_{i=N_1^*,N_2^*,\Delta,E} A_i \sum_{n=n_i^{min}}^{n_i^{max}} (1-x)^4$$
$$\cdot\, M_{i,n}(x,Q^2)\left(1 - 4\frac{Q^2_{0,i}+s-m_p^2}{Q^2} + O\left(\frac{1}{Q^4}\right)\right), \tag{33}$$

where

$$M_{i,n}(x,Q^2) = \frac{(s-m_p^2)x}{4\pi\alpha(1+\frac{4m_p^2x^2}{Q^2})}\left(\frac{Q^2_{0,i}}{s-m_p^2}\right)^4 \frac{\mathcal{I}m\ \alpha_i(s)}{(n - \mathcal{R}e\ \alpha_i(s))^2 + (\mathcal{I}m\ \alpha_i(s))^2}\ . \tag{34}$$

In our range of interest $M_{i,n}$ is a slowly varying function of both x and Q^2. For each (i,n) the term proportional to $(1-x)^{4(n-n_i^{max}+1)}$ shows the main tendency of $F_2(x,Q^2)_{i,n}$, while $M_{i,n}$ is responsible for the "fine structure" - resonances at large x. Of course, for each trajectory i the main contribution comes from the first resonance - $(1-x)^4$.

At this point it might be interesting to see the effect of spin corrections. As it has been shown in Ref. [28], if one explicitly takes into account the spin structure of the F_2, the main contribution from each resonance in the limit $x \to 1$ ($Q^2 \to \infty$) is proportional to $(1-x)^3$. Thus our model, neglected spin effects, strongly underestimate the physical SF. This might be another reason why the duality ration, Eq. (28), is so small in the high Q^2 region.

8 Conclusions

The idea of the present paper is that deep inelastic scattering can be described by a sum of direct channel resonances lying on Regge trajectories. The form of these trajectories is crucial for the dynamics. It is constrained by analyticity, unitarity and by the experimental data. The use of baryon trajectories instead of individual resonances not only makes the model economic (several resonances are replaced by one trajectory) but also helps in classifying the resonances, by including the "right" ones and eliminating those nonexistent.

Compton scattering of nuclei is much similar to πN scattering. The difference coming mainly from the photon spin imposes selection rules on inelastic transitions. These selection rules are approximate, and can be introduced either in the construction of the scattering amplitude (cross section, SF), or just by fitting the model to the data.

To fix the ideas and make a rough fit to the data, we constructed a simplified model with just 3 baryon trajectories, in which heavy thresholds have been replaced for simplicity by a linear term, and with the lowest-lying resonances. In fact, apart

from the "prominent" three resonances many more should be included by means of relevant baryon trajectories. To this end an independent study of baryon trajectories and updated fits to dozens of existing resonances should be done. We intend to continue working in this direction.

The dynamics of DIS can be described either by the contribution of direct-channel or cross-channel Regge trajectories.

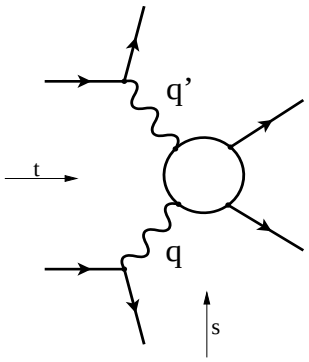

Figure 6: Typical six-point function ansatz.

An important issue of our paper is the integral representation realizing parton-hadron, or Bloom-Gilman duality. This can be seen from the equivalence of its pole decomposition (resonances) and smooth large-Q^2 scaling behavior. As a result, a Q^2- dependent photon Regge trajectory emerges. In the unphysical region of positive q^2 (negative Q^2), outside the one we consider, resonances are expected to appear on this trajectory. As it is known, these are the vector mesons $\rho, \omega, \phi, J/\Psi$ etc. The non-appearance of higher recurrences, with spin larger than 1, on the photon trajectory is a problem for linear photon trajectories. "Analytic" models of Regge trajectories used in our paper can resolve this problem: the real part of the photon trajectory is limited by $\mathcal{R}e\ \alpha_\gamma(Q^2) < 2$ and higher than spin one states are not expected there.

The dual model presented here is a part of a more general 6-point dual amplitude (see Fig. 6), where two pairs of external particles (electrons) are at a pole, corresponding to the photon trajectory $\alpha_\gamma(Q^2)$. Such a dual model, but without the important limitation $\mathcal{R}e\ \alpha_\gamma(Q^2) < 2$ and for $t = 0$, was considered in Ref. [31]. Relaxing the condition $t = 0$ one can apply the 6-point dual amplitude with the above trajectories to DIS in all possible kinematical regions, including off-diagonal or skew-symmetric (i.e. where $t \neq 0$) DIS. We intend to report on relevant results in a forthcoming publication.

Acknowledgments

We thank F. Paccanoni, E. Predazzi and B.V. Struminsky for fruitful discussions and I. Niculescu for a very useful and stimulating correspondence. L.J. and V.M., acknowledge the support from INTAS, grant 00-00366. A.F. and V.M. wish to thank the University of Calabria, where this work was completed, for the warm hospitality.

References

[1] M. Köbberling et al., Nucl. Phys. **82** (1974) 201.

[2] S. Stein et al., Phys. Rev. **12** (1975) 1884.

[3] F.W. Brasse et al., Nucl. Phys. **B110** (1976) 413.

[4] A. Bodek et al., Phys. Rev. **D20** (1979) 1471.

[5] L.J. Whitlow et al., Phys. Lett. **B250** (1990) 193.

[6] T.H. Bauer et al., Rev. Mod. Phys. **50** (1978) 261.

[7] P. Stoler, Phys. Rev. **D44** (1991) 73; Phys. Rev. Lett. **66** (1991) 1003.

[8] I. Niculescu, Ph.D. Thesis, Hampton University, May 1999.

[9] C.E. Carlson, N.C. Mukhopadhyaya, Phys. Rev. Lett. **74** (1995) 1288; Phys. Rev. **D58**(1998) 094029; Eur. Phus. J **C**, in press.

[10] C.E. Carlson and J.L. Poor, Phys. Rev. **D38**(1988) 2758; X. Ji and P. Unrau, Phys. Rev. **D52** (1995) 72.

[11] G. Sterman and P. Stoler, Ann. Rev. Nucl. Part. Sci. **47** (1997) 193.

[12] C.E Carlson, N.C. Mukhopadhyay, Phys. Rev. **D58** (1998) 094029; X. Ji and W. Melnitchouk, Phys. Rev. **D56** (1997) 1; D. Qing and I. Schmidt, hep-ph/0106225; V.D. Burkert, nucl-ex/0108023, nucl-ex/0109004.

[13] I. Niculescu et al., Phys. Rev. Lett. **85** (2000) 1182; *ibid.* 1186.

[14] C.S. Armstrong et al., hep-ph/0104055.

[15] R. Ent, C.E. Koppel, I. Niculescu, Phys. Rev. **D62** (2000) 073008.

[16] S. Simula, Phys. Lett. **B481** (2000). 14.

[17] L.L. Jenkovszky, V.K. Magas, E. Predazzi, Eur. Phys. J. **A12** 361 (2001).

[18] L.L. Jenkovszky, V.K. Magas, E. Predazzi, nucl-th/0110085; L.L. Jenkovszky, V.K. Magas, hep-ph/0111398; L.L. Jenkovszky, T. Korzhinskaja , V.I. Kuvshinov and V.K. Magas, Proceedings of the New Trend in High-Energy Physics, Yalta, Crimea, Ukraine, September 22-29, 2001, edited by P.N. Bogolyubov and L.L. Jenkovszky (Bogolyubov Institute for Theoretical Physics, Kiev, 2001), p. 178.

[19] L.L. Jenkovszky, V.K. Magas and T. Szabo, Proceedings of the International Worshop on Very High Mulitiplicities, Dubna, Russia, 7-9 April 2001, in press.

[20] R. Fiore, L. Jenkovszky, V. Magas, F. Paccanoni and A. Papa, Eur. Phys. J. **A10** 217 (2001); Nucl. Phys. Proc. Suppl. **99** 68 (2001).

[21] P. Freund, Phys. Rev. Lett. **20**, (1968) 235; H. Harari, Phys. Rev. Lett. **20**, (1968) 1395.

[22] G. Domokos, S. Kövesi-Domokos, E. Schoenberg, Phys. Rev. **3** (1971) 1184.

[23] F. Halzen and A.D. Martin. *Quarks & Leptons: An Introductory Course in Modern Particle Physics*, John Wiley & Sons, 1984; F.E. Close. *An Introduction to Quarks and Partons.* Academic Press, 1979.

[24] P.D.B. Collins, *Introduction to Regge Theory and High Energy Physics*, University Press, 1977.

[25] A. Bugrij et al., Fortschritte der Physik, **21**, (1973) 427.

[26] V. Magas, Ukr. Fiz. Zh. **44** (1999) 438; R. Fiore, L. L. Jenkovszky, V. K. Magas and F. Paccanoni, Phys. Rev. **D60** (1999) 116003.

[27] Particle Data Group, Eur. Phys. J. **C3** (1998) 1.

[28] V.V. Davydovsky and B.V. Struminsky, hep-ph/0205130.

[29] http://www.jlab.org/resdata.

[30] L. Csernai, L. Jenkovszky, K. Kontros, A. Lengyel, V. Magas and F. Paccanoni, hep-ph/0112265, DOI 10.1007/s100520200931.

[31] F. Schierholz and M.G. Schmidt, Phys. Rev. **D10**(1974) 175.

Table 1: Parameters of the fit. In the first coloumn we show the result of the fit when the parameters of the barionic trajectories are fixed. The second coloumn contains the result of the fit when the parameters of the trajectories are varied. † - parameters of the physical baryon trajectories from Eqs. (16-18). * - the coefficient $norm$ is chosen in such a way as to keep $A_{N_1^*} = 1$ in order to see the interplay between different resonances.

N_1^*	α_0	-0.8377 (fixed)†	-0.8070
	α_1	0.95 (fixed)†	0.9632
	α_2	0.1473 (fixed)†	0.1387
	$A_{N_1^*}$	1 (fixed)*	1 (fixed)*
	$Q^2_{N_1^*}$, GeV^2	2.4617	2.6066
N_2^*	α_0	-0.37(fixed)†	-0.3640
	α_1	0.95 (fixed)†	0.9531
	α_2	0.1471 (fixed)†	0.1239
	$A_{N_2^*}$	0.5399	0.6086
	$Q^2_{N_2^*}$, GeV^2	2.9727	2.6614
Δ	α_0	0.0038 (fixed)†	-0.0065
	α_1	0.85 (fixed)†	0.8355
	α_2	0.1969 (fixed)†	0.2320
	A_{Δ}	4.2225	4.7279
	Q^2_{Δ}, GeV^2	1.5722	1.4828
	s_0, GeV^2	1.14 (fixed)†	1.2871
E	α_0	0.5645	0.5484
	α_2	0.1126	0.1373
	s_E, GeV^2	1.3086	1.3139
	A_{exot}	19.2694	14.7267
	Q^2_{exot}, GeV^2	4.5259	4.6041
	$norm$	0.021	0.0207
$\chi^2_{d.o.f.}$		28.29	11.60

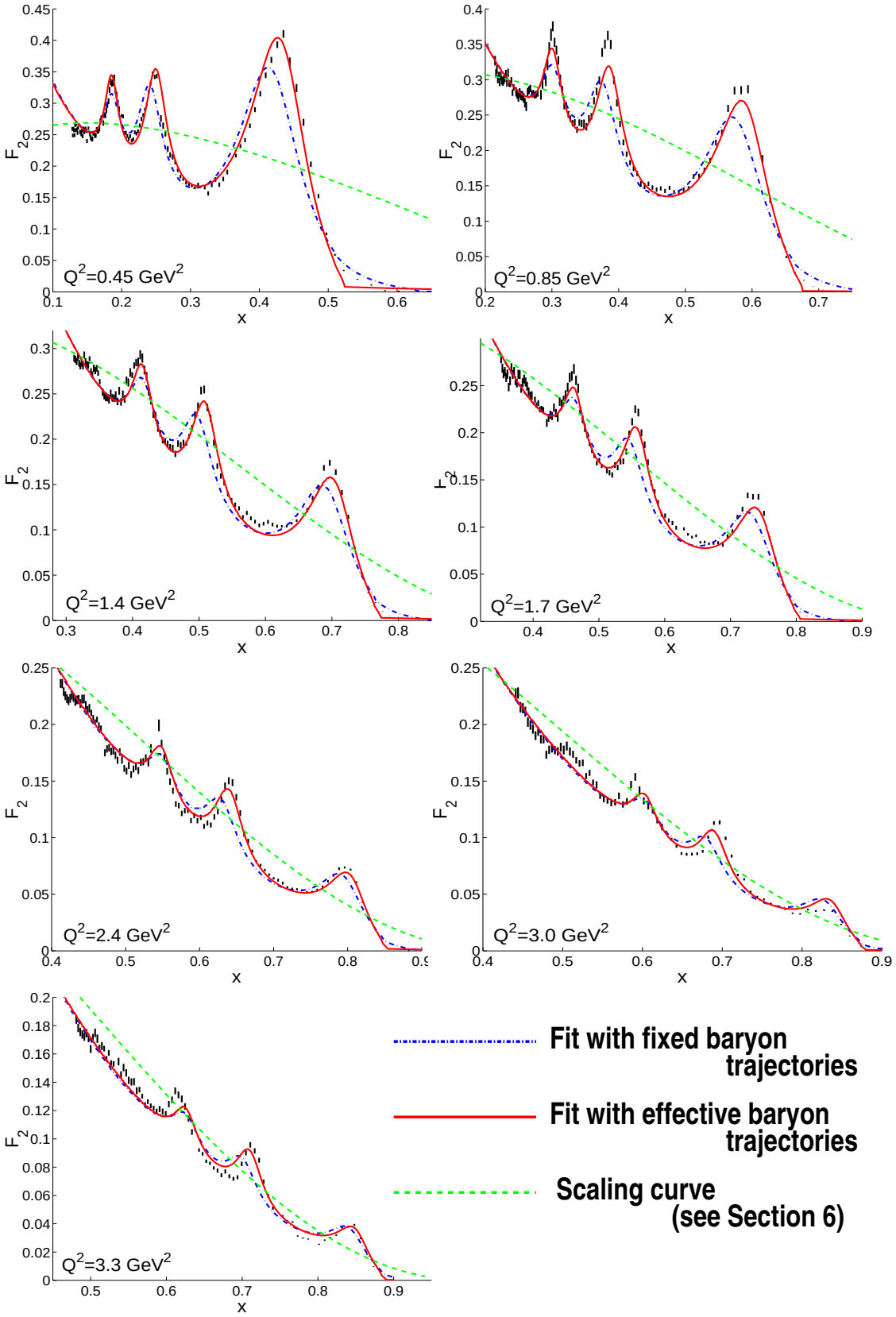

Figure 7: F_2 as a function of x for $Q^2 = 0.45 - 3.3$ GeV^2.